Neutral Hydrogen and the Infrared Connection

HIPASS / WHISP / ALFALFA \\ WISE







Thomas Jarrett (Cape Town)

+ visualisation nuggets

Mid-IR <> SF <> Gas

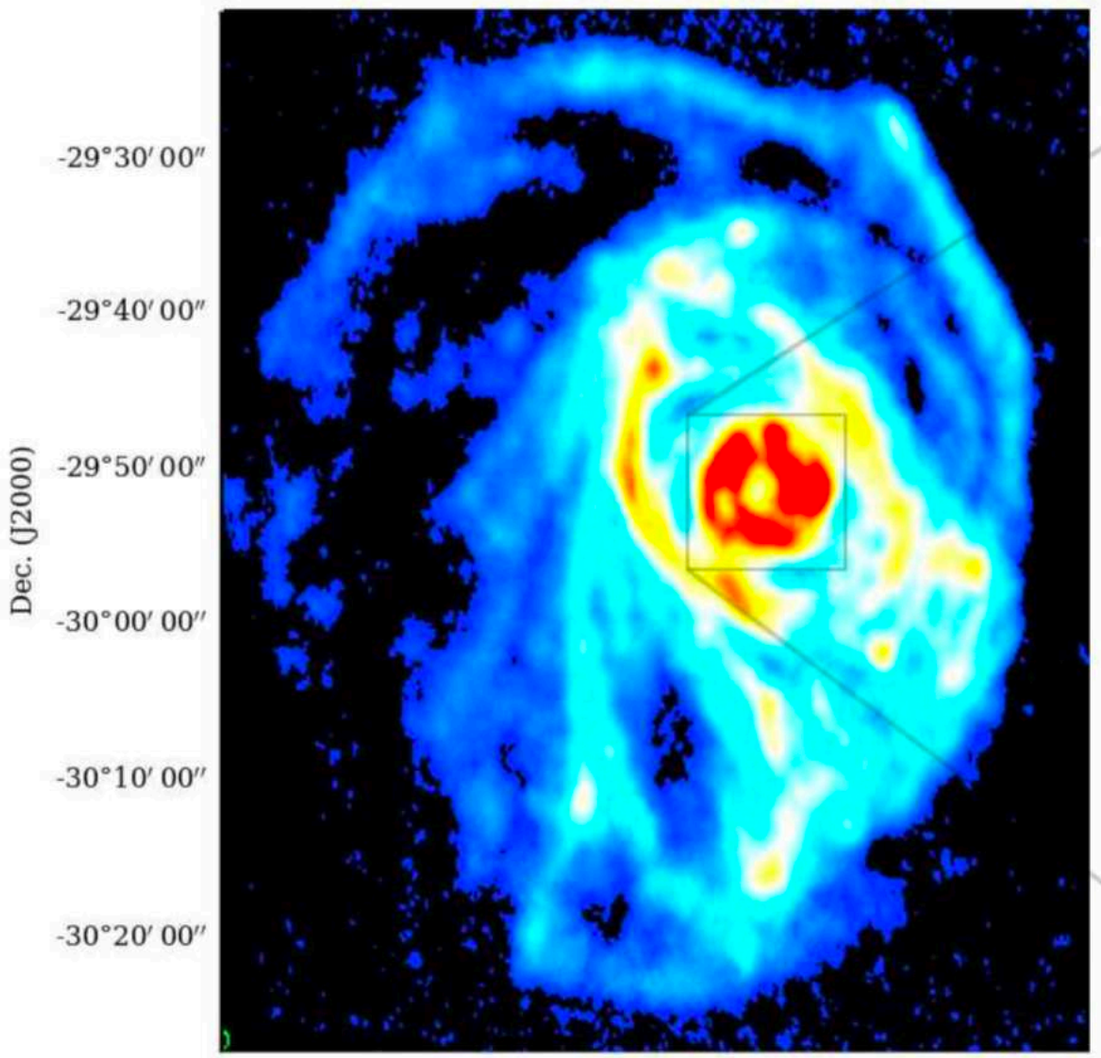

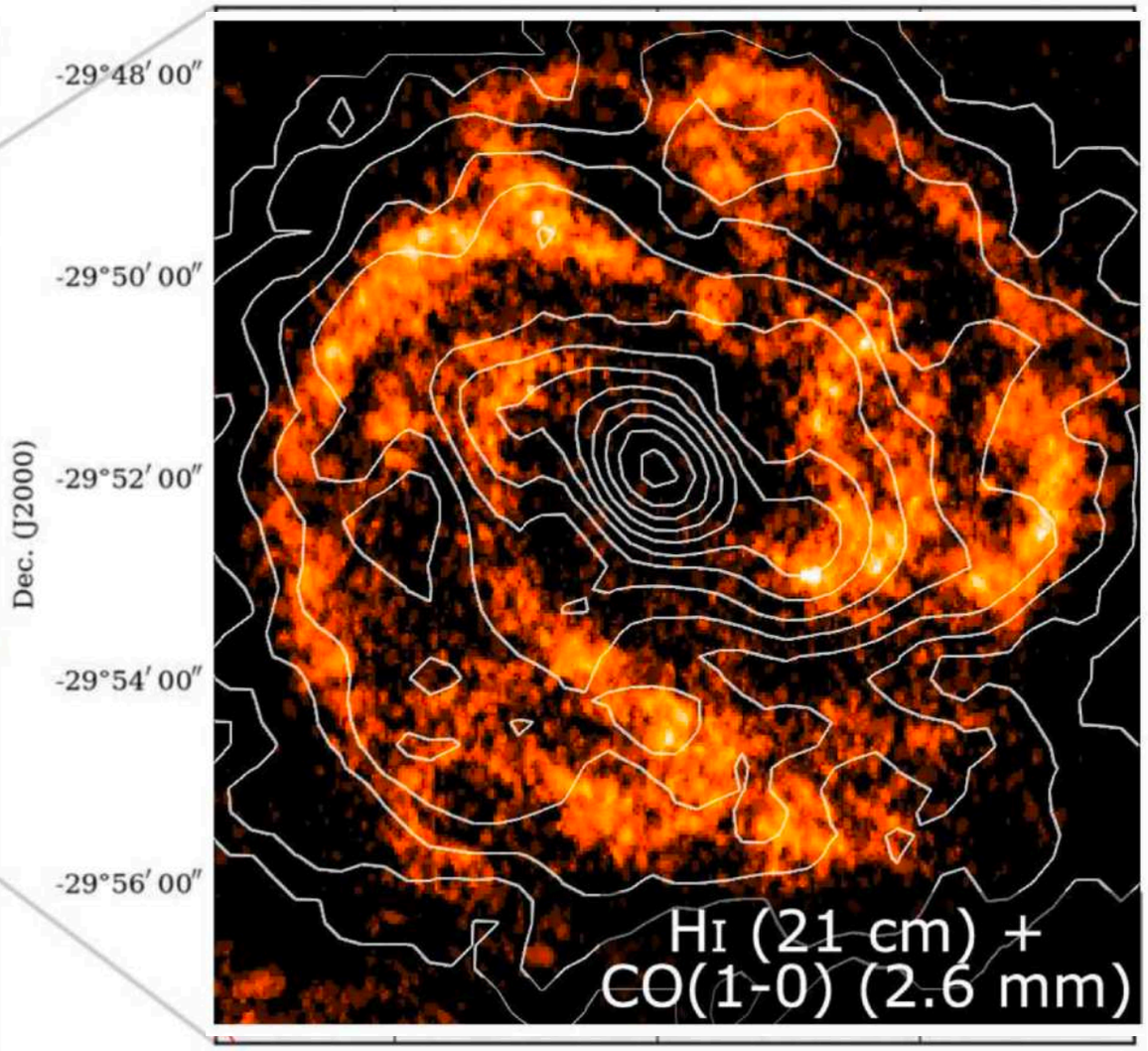

HI

LVIS ; Koribalski

WISE 12 μm

Jarrett+2013

Mid-IR <> TIR <> SF

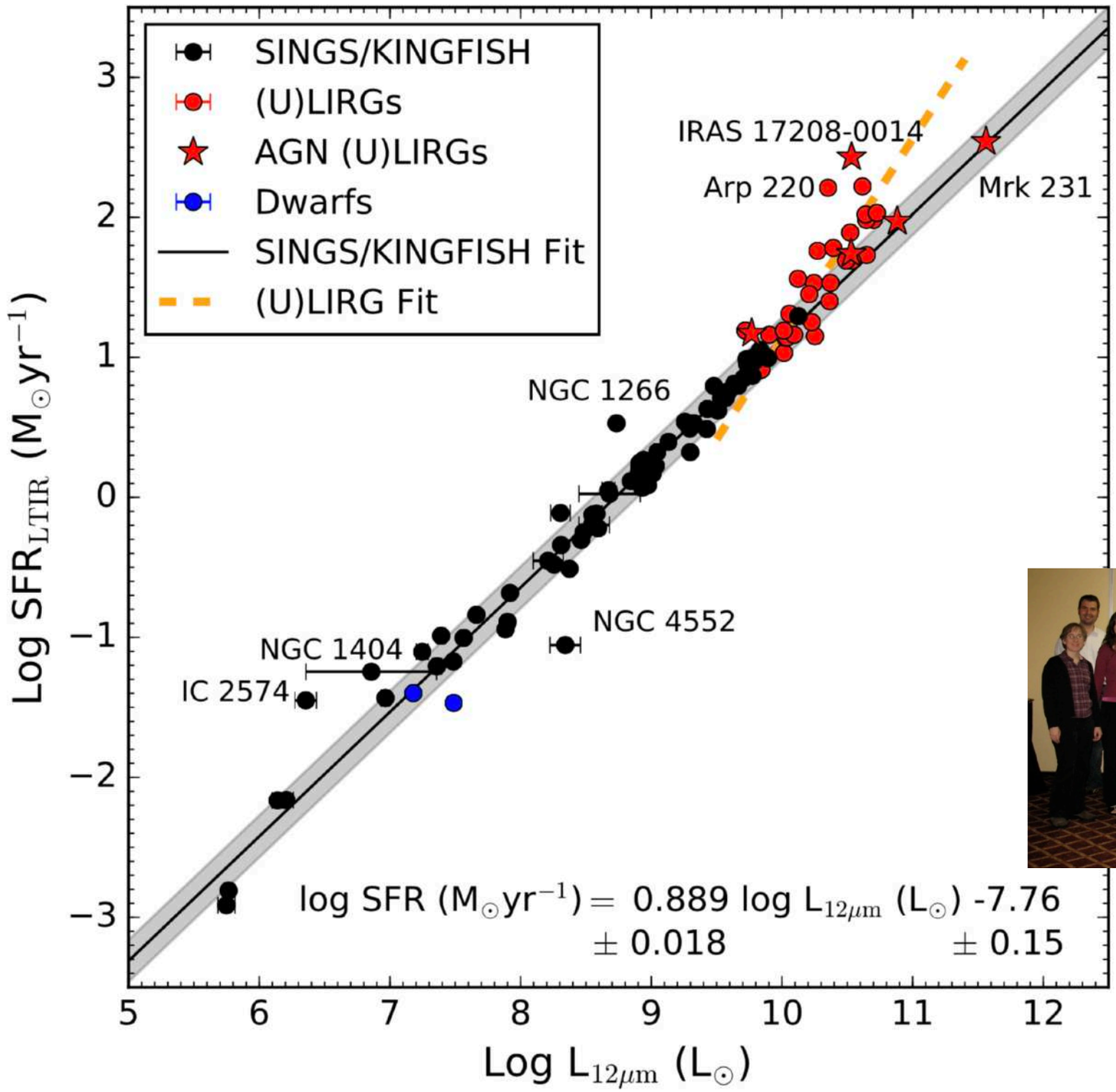

SINGS

KINGFISH

Cluver+2017 (ApJ, 850, 68)

RELATIONSHIPS BETWEEN HI GAS MASS, STELLAR MASS AND STAR FORMATION RATE OF HICAT+WISE (HI-WISE) GALAXIES

Vaishali Parkash,[1] Michael J. I. Brown,[1] T. H. Jarrett,[2] and Nicolas J. Bonne[3]

Parkash+2018 (ApJ, 864, 40)

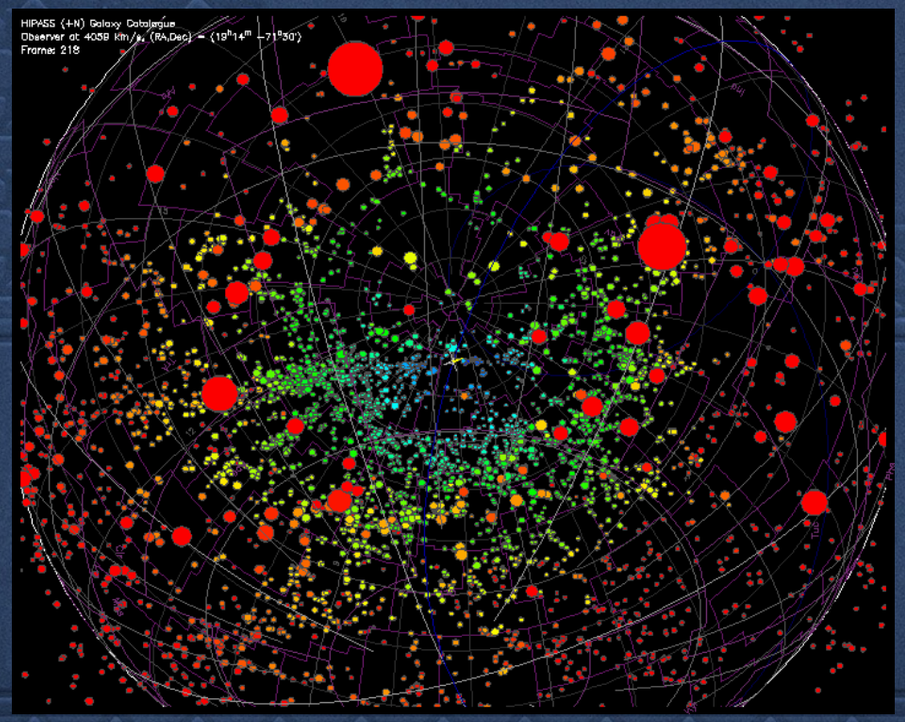

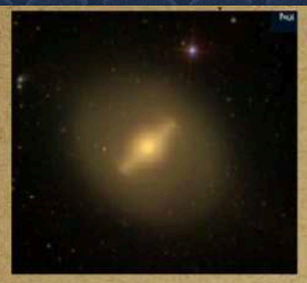

Spiral Sample

- **Main sources of data: HIPASS (HI) + WISE (stellar mass and SFR).**
- **New WISE photometry**
- **Morphologies and redshifts from prior literature (e.g., Bonne et al. 2015).**
- **All spiral galaxies (t-type ≥ 0) in the southern hemisphere with z < 0.01 & w1 (3.4μm) < 10 mag**
- **High HI Detection Completeness: 548/ 585 (94%, 433 HIPASS sources + 115 from the literature (Paturel et al. (2003), Huchtmeier & Richter (1989), Springob et al. (2005) and Masters et al. (2014).)**

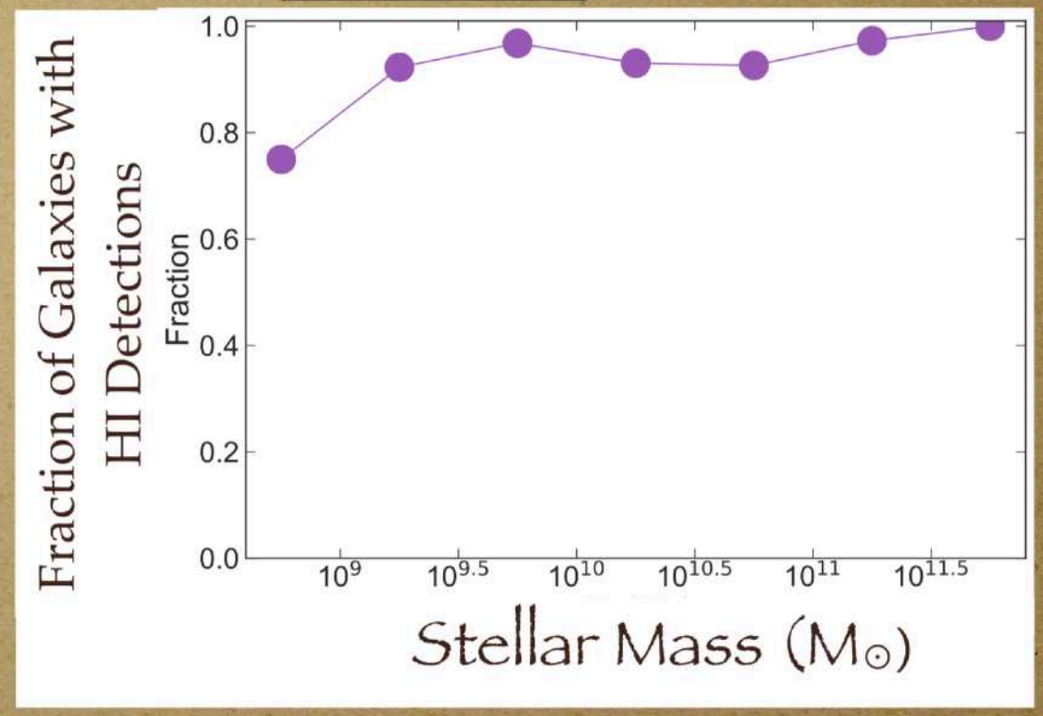

Parkash+2018 (ApJ, 864, 40)

HI mass vs Stellar Mass

- The median H I mass increases with stellar mass with a least-squared fit of

$$\log M_{HI} = 0.35\,(\log M_* - 10) + 9.45$$

- At a given stellar mass the median H I mass increases with T-type while the dispersion decreases with T-type. Serra et al (2012) suggests this scatter of HI masses with decreasing T-type reflects the large variety of HI content of early-type galaxies, and confirms the lack of correlation between HI mass and luminosity.

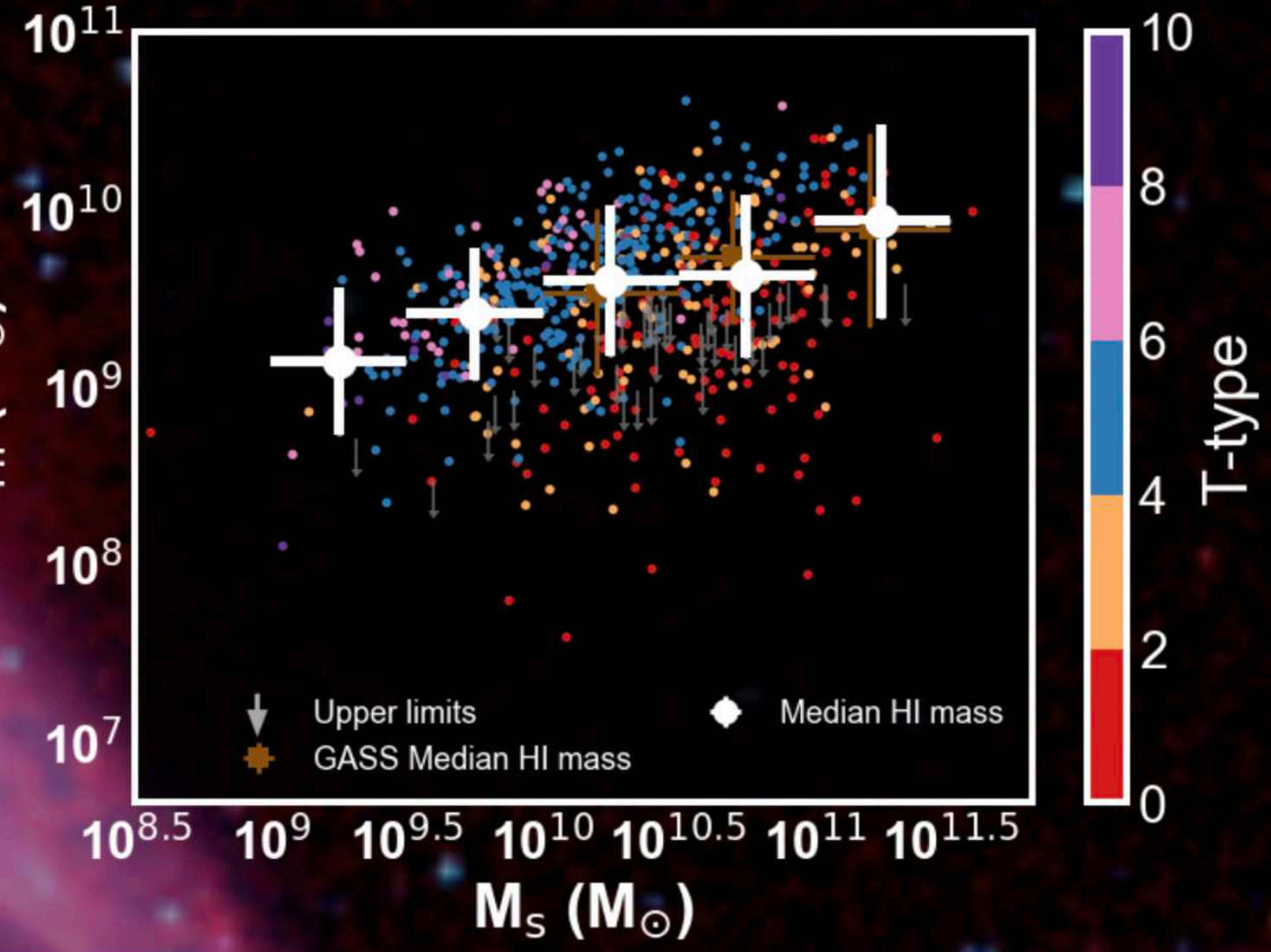

Parkash+2018 (ApJ, 864, 40)

Upper Limit to HI Mass?

- Obreschkow et al. (2016) shows that the fraction of neutral atomic gas in isolated local disk galaxies of baryonic mass M is well described by a straightforward stability model for flat exponential disks and the halo spin parameter.

- The angular momentum of a dark matter halo is parameterised through the spin parameter:

$$\lambda \equiv \frac{J_{halo} E_{halo}^{1/2}}{G M_{halo}^{5/2}}$$

- For isolated local disk galaxies the fraction of atomic gas

$$f_{atm} = \min\left\{1,\ 0.5\left(\frac{\lambda}{0.03}\right)^{1.12}\left(\frac{M}{10^9 M_\odot}\right)^{-0.37}\right\}$$

- The median HI-stellar mass distribution is in good agreement with the expected mean f_{atm} ($\lambda = 0.035$). The observed upper limit is consistent with the predicted HI-stellar mass curve for the upper limit for λ (= 0.112). This is consistent with the hypothesis that the maximum HI fraction is set by that of the halo spin parameter.

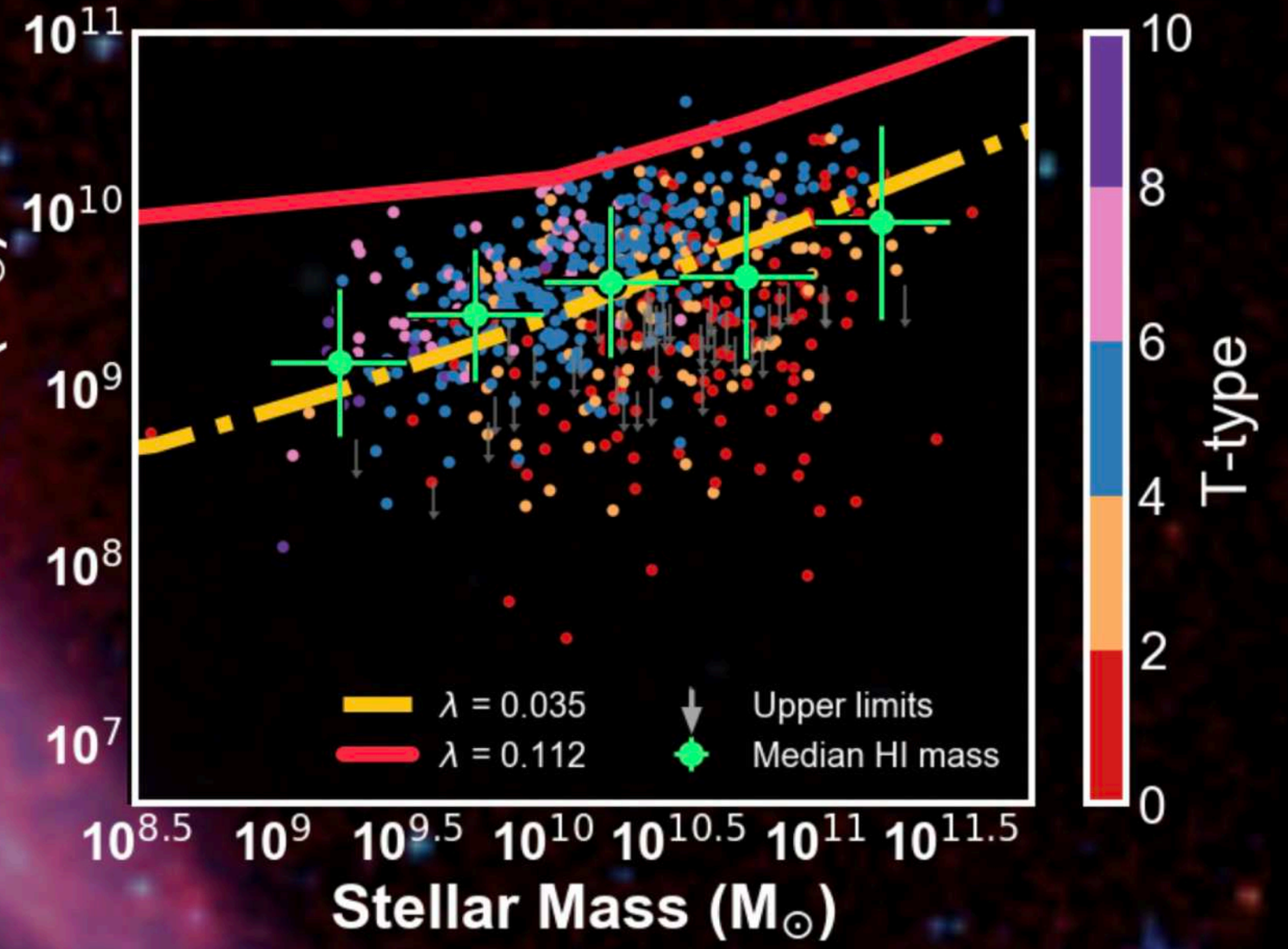

Parkash+2018 (ApJ, 864, 40)

Star Forming Main Sequence

- The changing trend of SFR with increasing stellar mass and the increased dispersion of SFRs is evidence of mass quenching, and this also coincides with an increasing fraction of early-type spirals (T-type ≤ 2).

- To mitigate the effect of mass-quenching on our model fit to MS, we only fit to galaxies with stellar mass ≤ $10^{10.5}$ $M_\odot$ and measure the MS to be

$$\log\ \mathrm{SFR} = 0.7\ (\log\ M_* - 10) - 0.09$$

- Measured the SFE of spiral galaxies to be constant at $10^{-9.57}$ yr^{-1} ± 0.4 dex for 2.5 orders of magnitude in stellar mass, despite the higher stellar mass spirals showing evidence of quenched star formation.

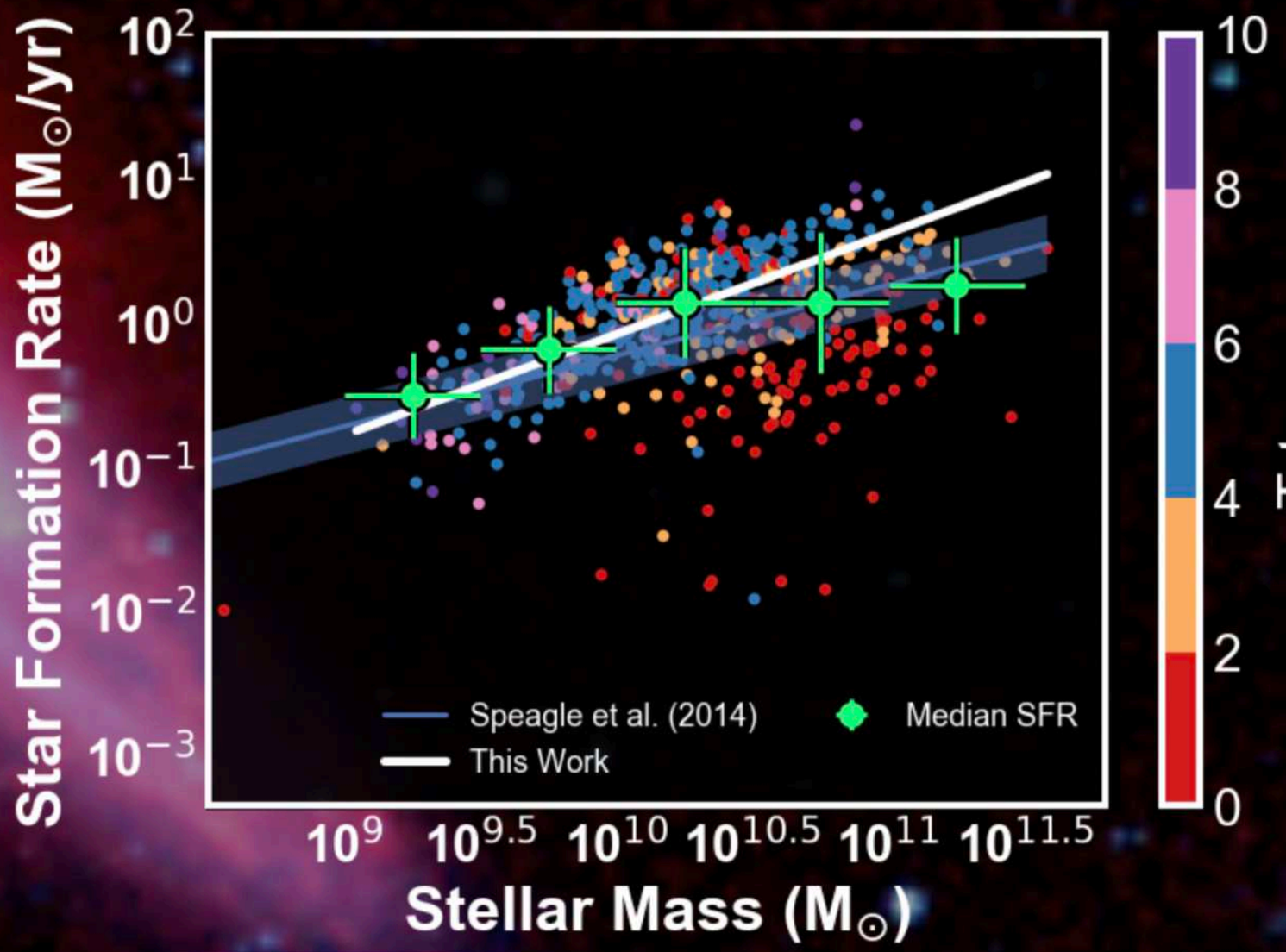

Parkash+2018 (ApJ, 864, 40)

Star Formation Efficiency

- Measured the SFE of spiral galaxies to be constant at $10^{-9.57}$ yr^{-1} ± 0.4 dex for 2.5 orders of magnitude in stellar mass, despite the higher stellar mass spirals showing evidence of quenched star formation.

- HI-selected samples show that SFE increases with stellar mass, but this is an artifact of excluding low H I mass galaxies. Stellar mass-selected samples, on the other hand, show that SFE is constant with stellar mass.

- Why is SFE constant?

- Wong et al. (2016) finds the constant SFE can be described by a model of the marginally stable disk coupled with hydrostatic pressure prescription for estimating the SFE and molecular-to-atomic ratio.

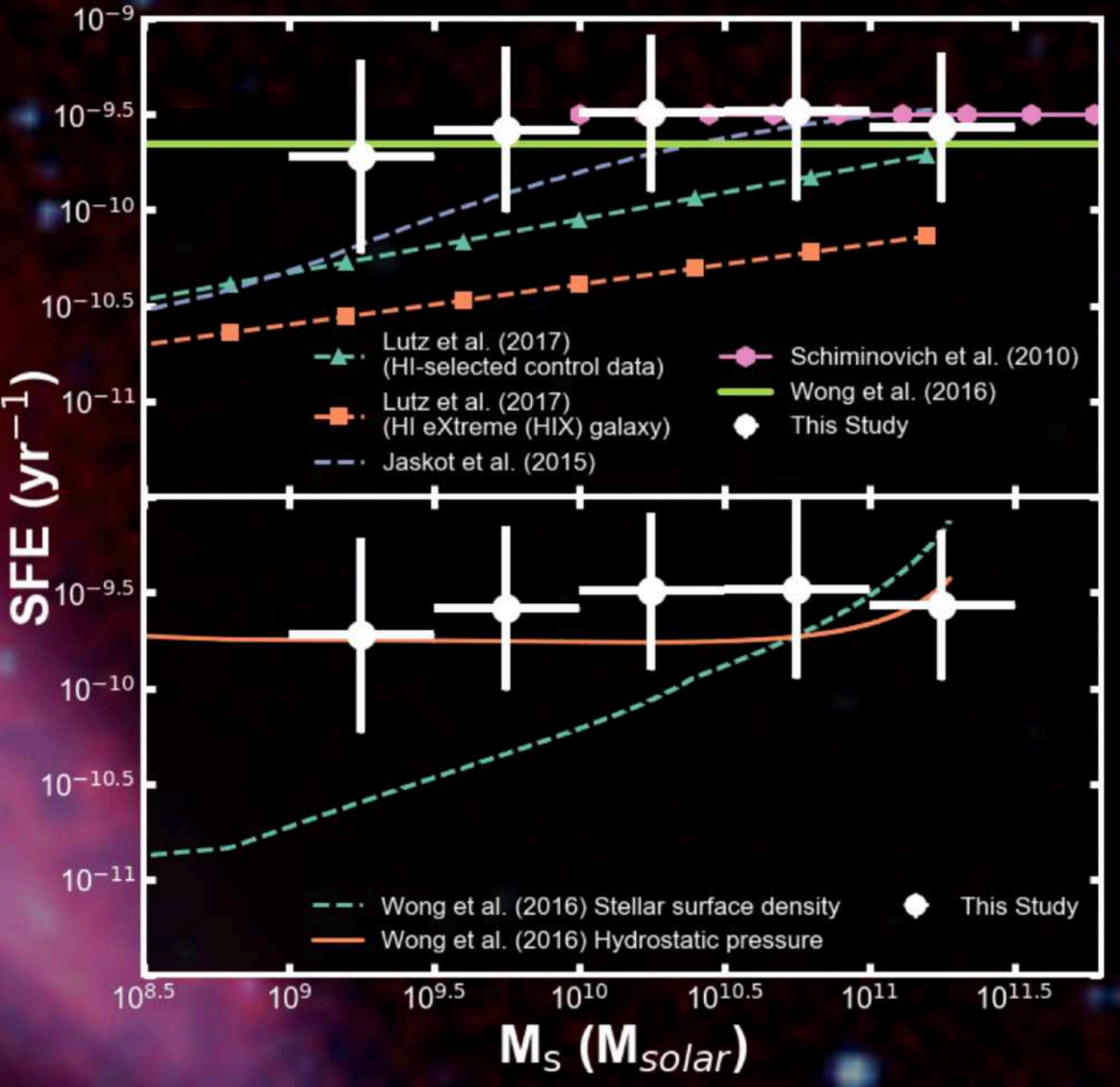

Parkash+2018 (ApJ, 864, 40)

Star formation thresholds in nearby galaxies

Elizabeth Naluminsa

UGC7766

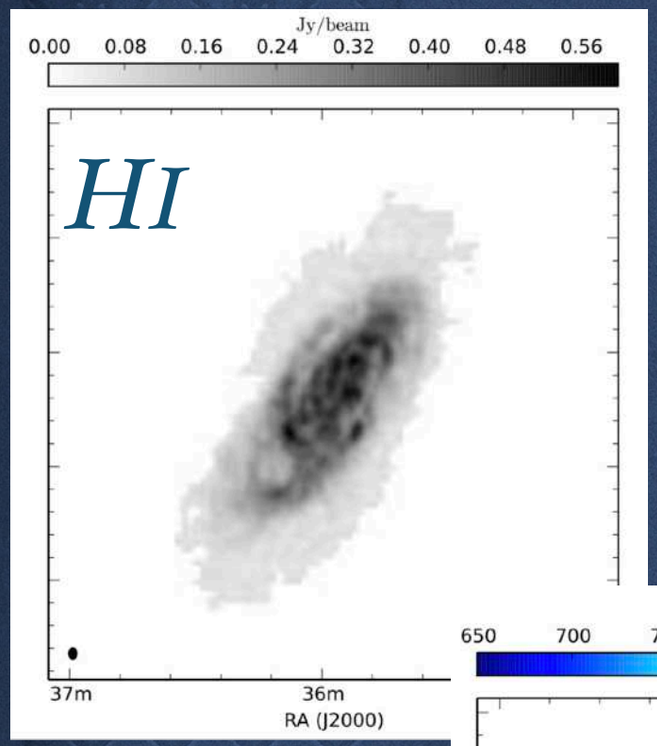

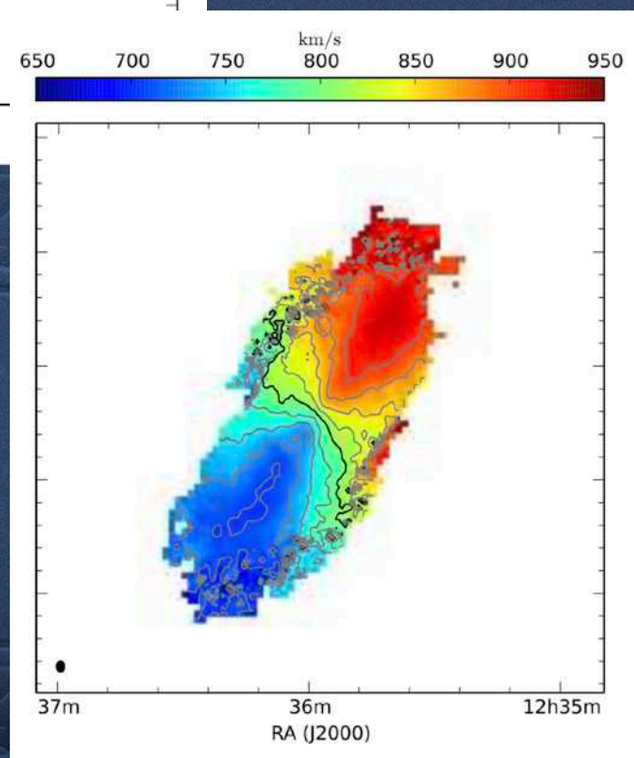

WHISP

WISE

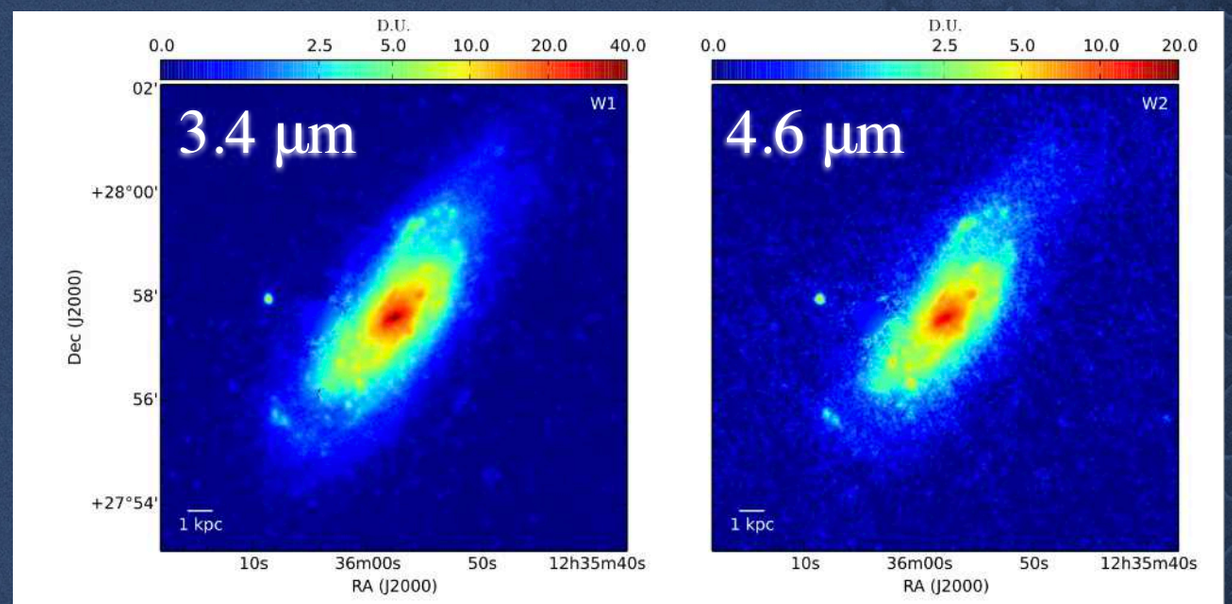

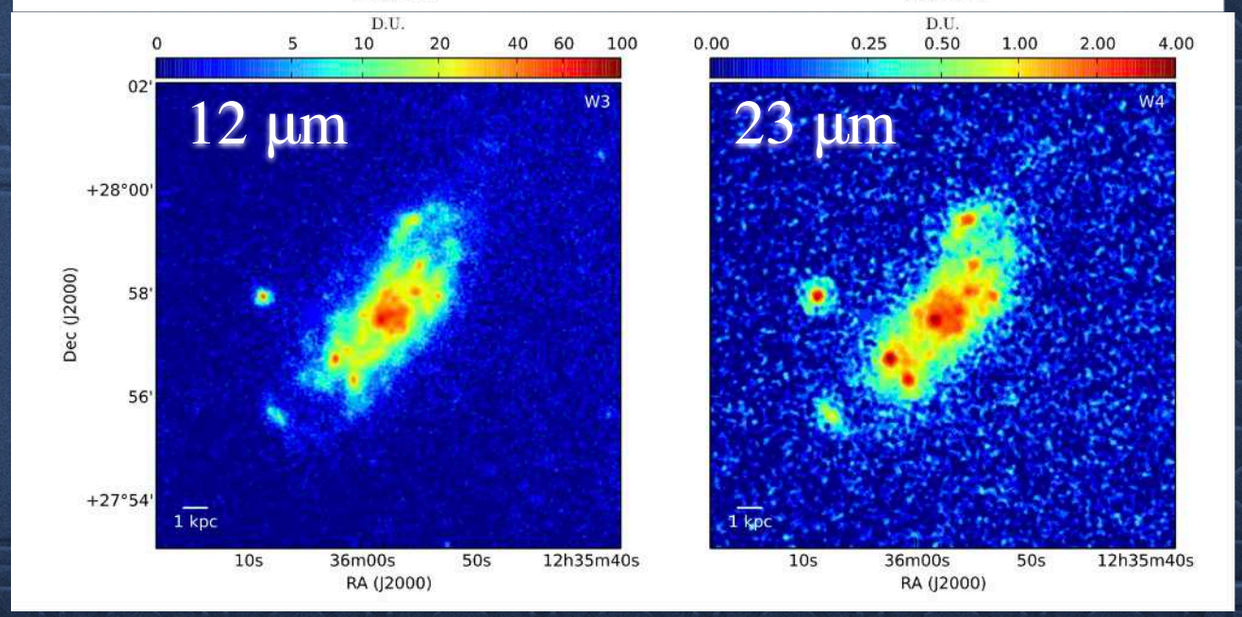

SF Thresholds

$$Q = \frac{\sigma_g \kappa}{\pi G \Sigma_g} < 1,$$

$$\Sigma_c = \alpha \frac{\sigma_g \kappa}{\pi G},$$

Toomre (1964)

Kennicutt (1989)

single

$$\frac{2\pi G k \Sigma_{*,o}}{\kappa^2 + k^2 \sigma_*^2} + \frac{2\pi G k \Sigma_{g,o}}{\kappa^2 + k^2 \sigma_g^2} > 1,$$

$$\frac{1}{Q_{sg}} = \frac{2}{Q_*} \frac{q}{1+q^2} + \frac{2}{Q_g} R \frac{q}{1+q^2 R^2} > 1,$$

Jog & Solomon (1984b)

Rafikov (2001)

double

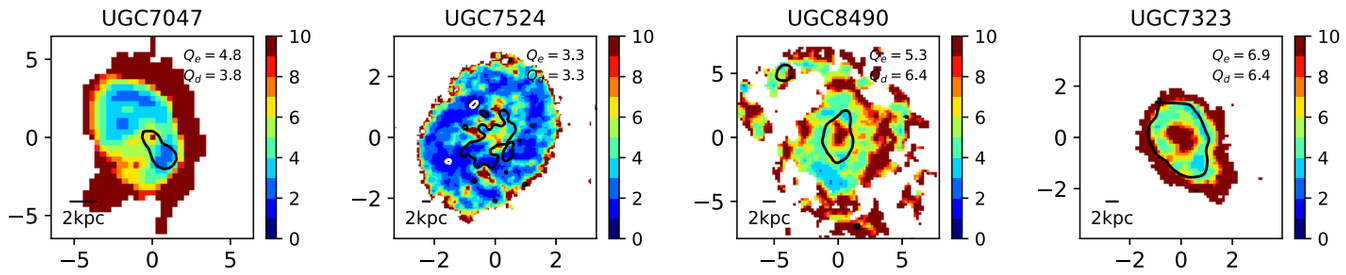
UGC7047
$Q_e = 4.8$
$Q_d = 3.8$
UGC7524
$Q_e = 3.3$
$Q_d = 3.3$
UGC8490
$Q_e = 5.3$
$Q_d = 6.4$
UGC7323
$Q_e = 6.9$
$Q_d = 6.4$
2kpc

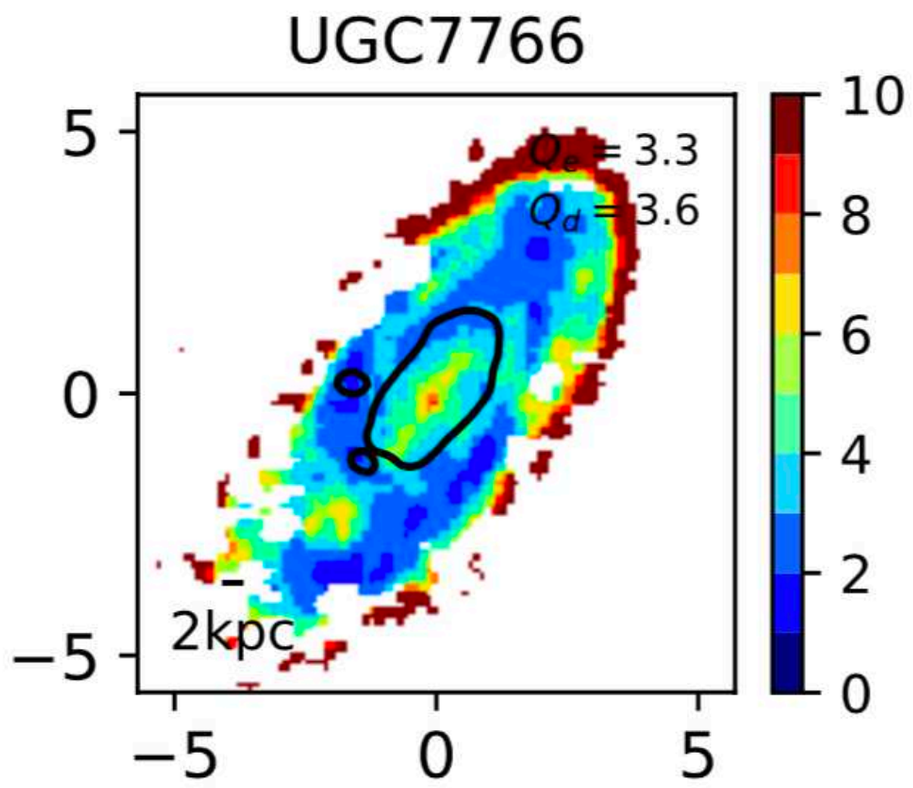
UGC7766
$Q_e = 3.3$
$Q_d = 3.6$
2kpc
R/Re

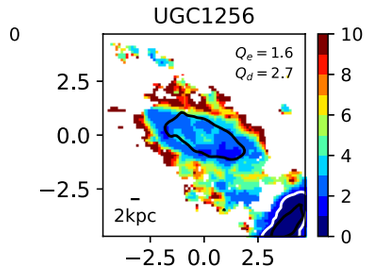
UGC1256
$Q_e = 1.6$
$Q_d = 2.7$
2kpc

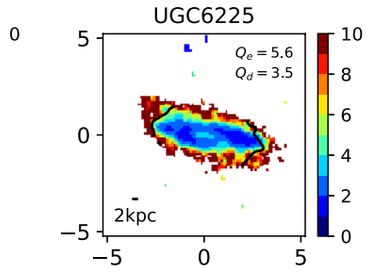
UGC6225
$Q_e = 5.6$
$Q_d = 3.5$
2kpc

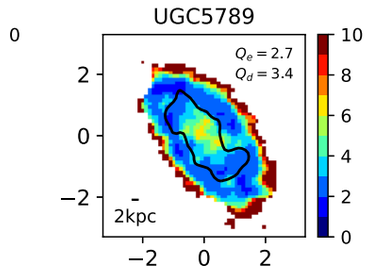
UGC5789
$Q_e = 2.7$
$Q_d = 3.4$
2kpc

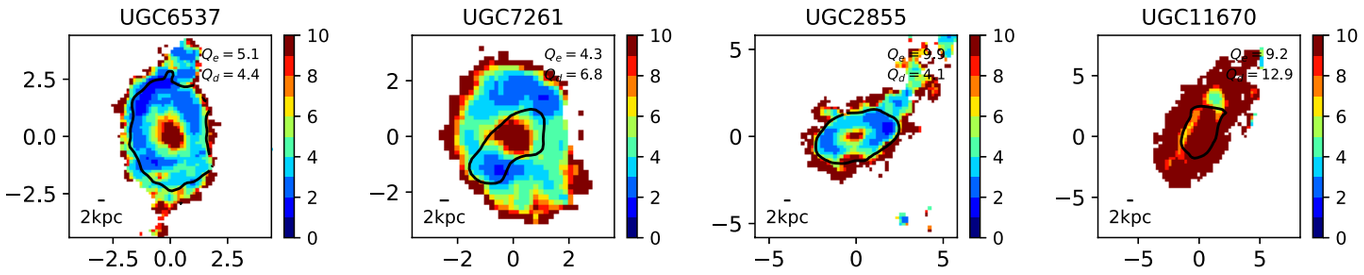
UGC6537
$Q_e = 5.1$
$Q_d = 4.4$
UGC7261
$Q_e = 4.3$
$Q_d = 6.8$
UGC2855
$Q_e = 9.9$
$Q_d = 4.1$
UGC11670
$Q_e = 9.2$
$Q_d = 12.9$
2kpc

R/Re

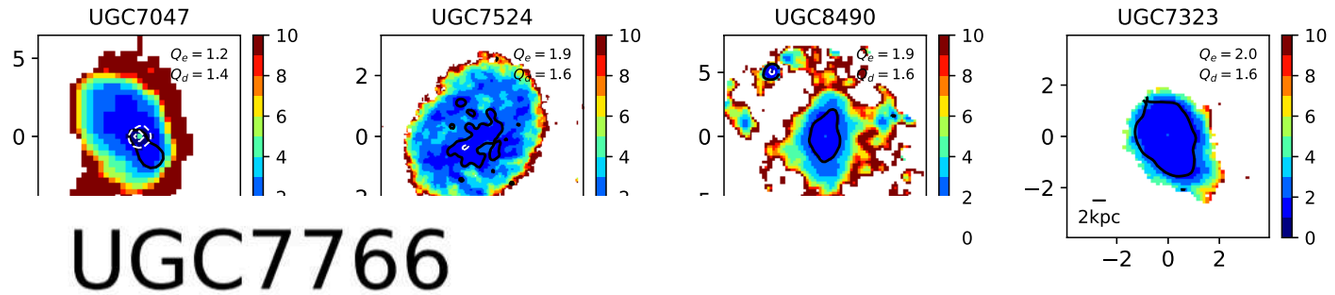
UGC7047
$Q_e = 1.2$
$Q_d = 1.4$
UGC7524
$Q_e = 1.9$
$Q_d = 1.6$
UGC8490
$Q_e = 1.9$
$Q_d = 1.6$
UGC7323
$Q_e = 2.0$
$Q_d = 1.6$
2kpc

UGC7766

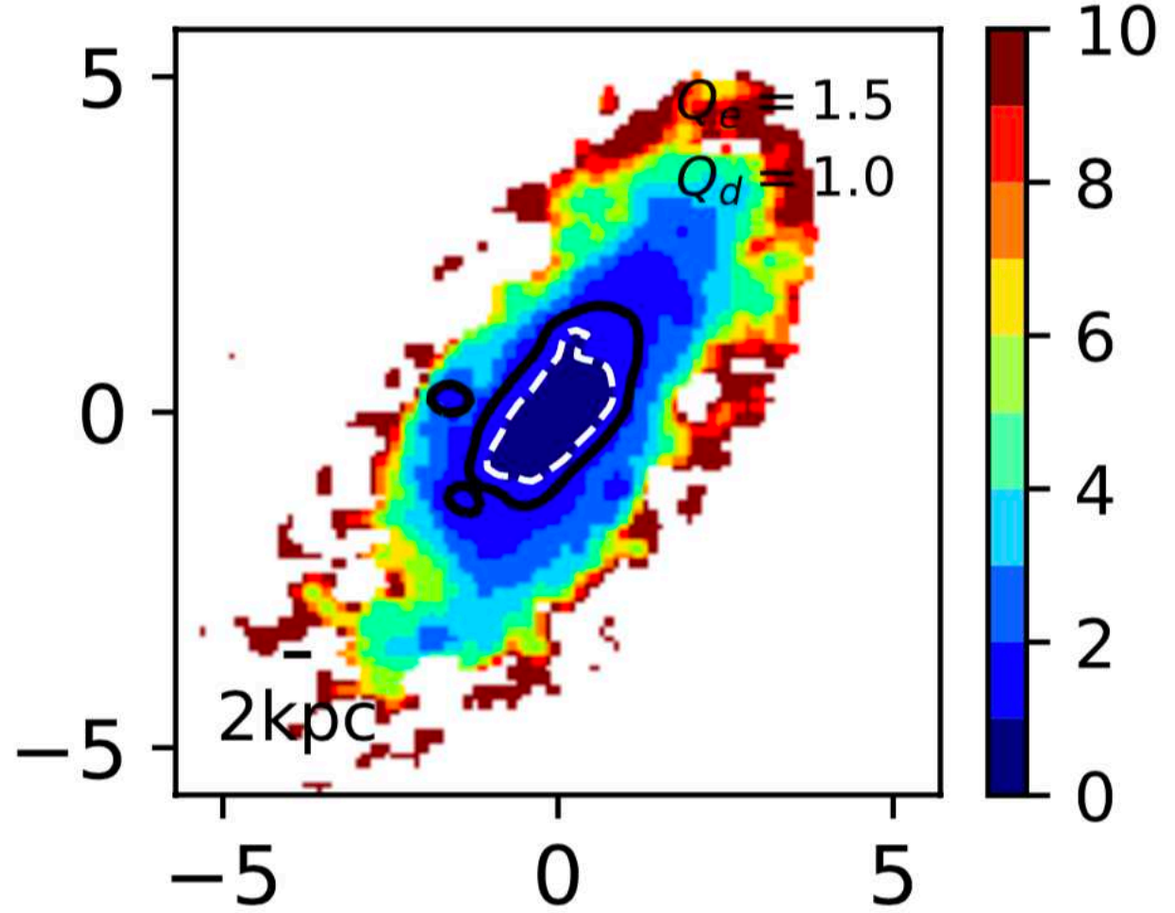
$Q_e = 1.5$
$Q_d = 1.0$
2kpc
R/Re

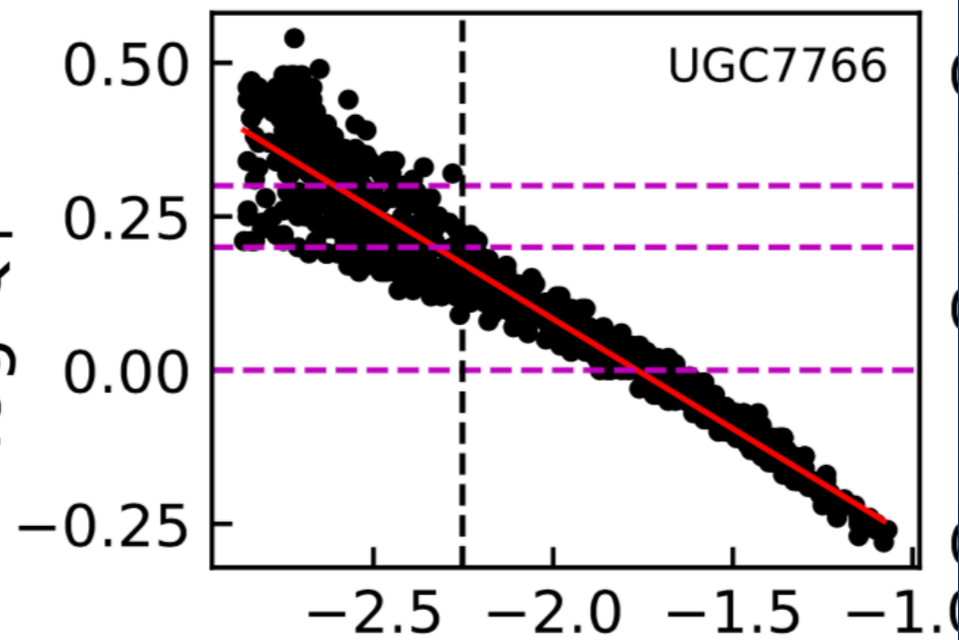
UGC7766
log Q_T
log $\Sigma_{SFR}[M_\odot yr^{-1}kpc^{-2}]$

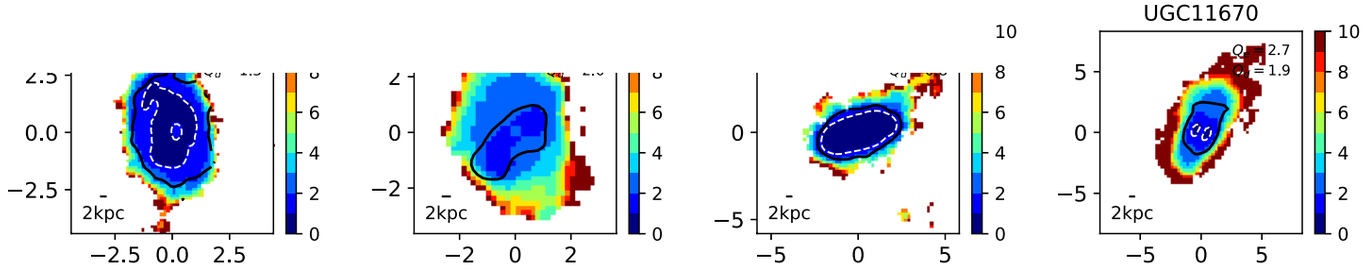
UGC11670
$Q_e = 2.7$
$Q_d = 1.9$
2kpc
R/Re

The role of HI & environment on the galaxy star formation rate-stellar mass sequence turnover

Jamie Bok

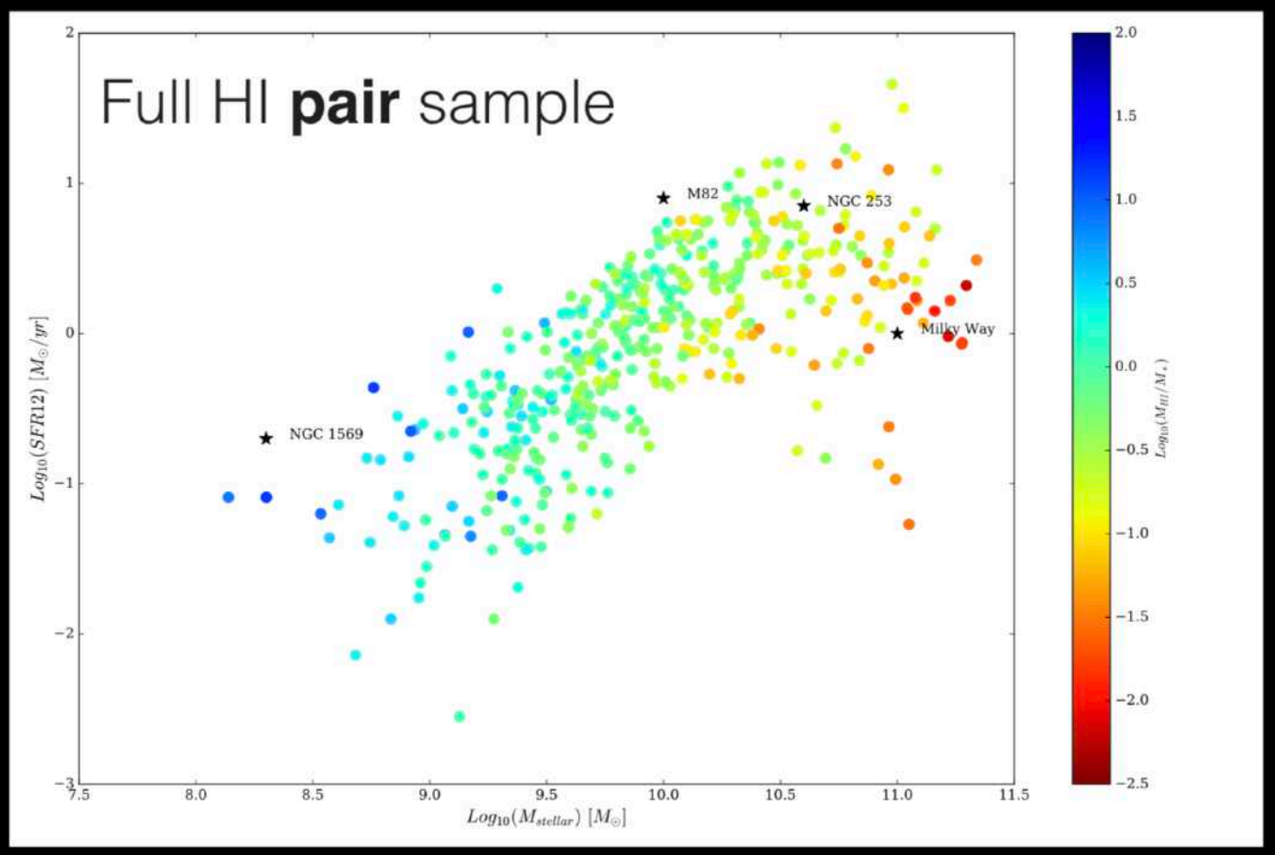

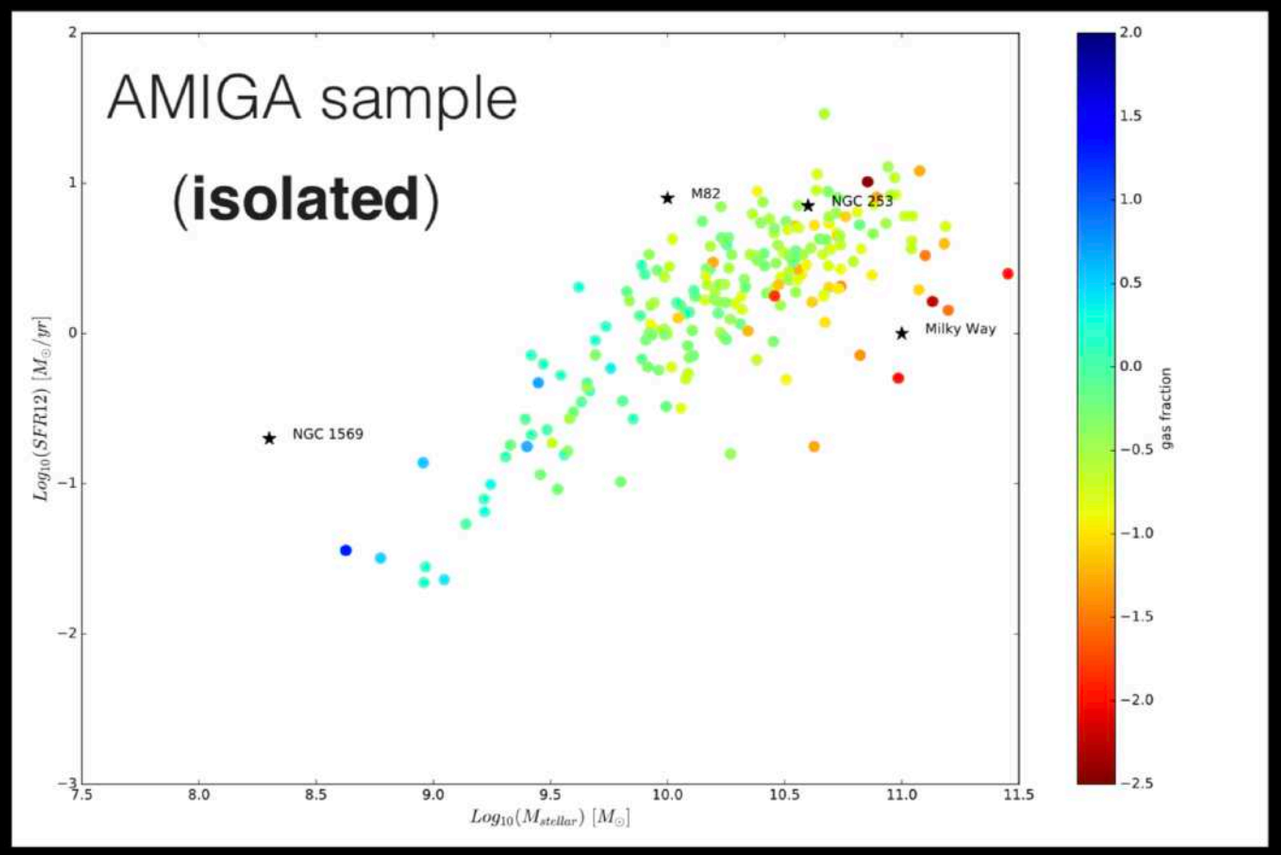

‘gas fraction log(MHI/M★)

Visualization

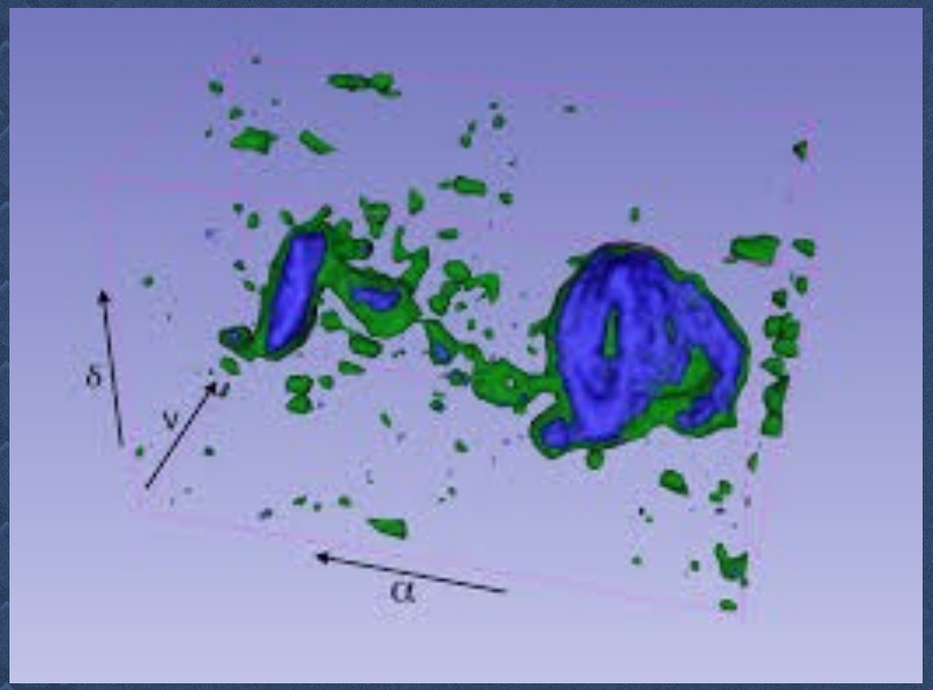

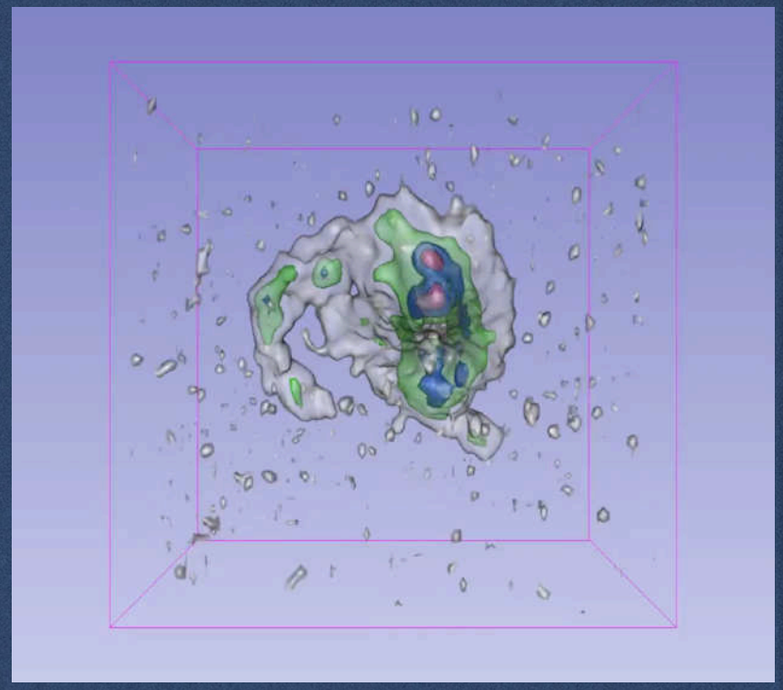

The role of 3-D interactive visualization in blind surveys of H I in galaxies

D. Punzo[a,*], J.M. van der Hulst[a], J.B.T.M. Roerdink[b], T.A. Oosterloo[a,c], M. Ramatsoku[a], M.A.W. Verheijen[a]

[a] *Kapteyn Astronomical Institute, University of Groningen, P.O. Box 800, 9700 AV Groningen, The Netherlands*
[b] *Johann Bernoulli Institute for Mathematics and Computer Science, University of Groningen, Nijenborgh 9, 9747AG Groningen, The Netherlands*
[c] *ASTRON, the Netherlands Institute for Radio Astronomy, Postbus 2, 7990 AA, Dwingeloo, The Netherlands*

Large walls & curved (immersive) screens

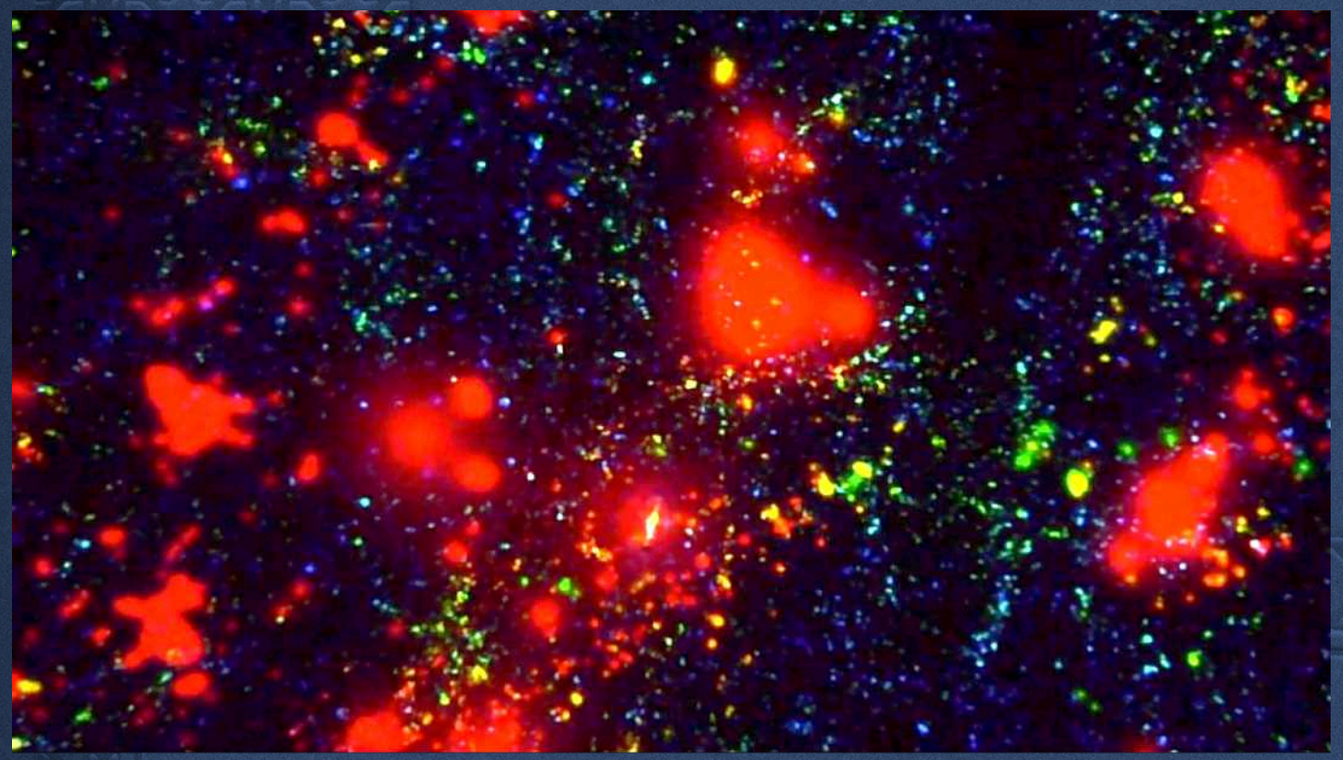

Astro VR

Galaxy-Galaxy Interaction (Nathan Deg 2018)

Astro VR

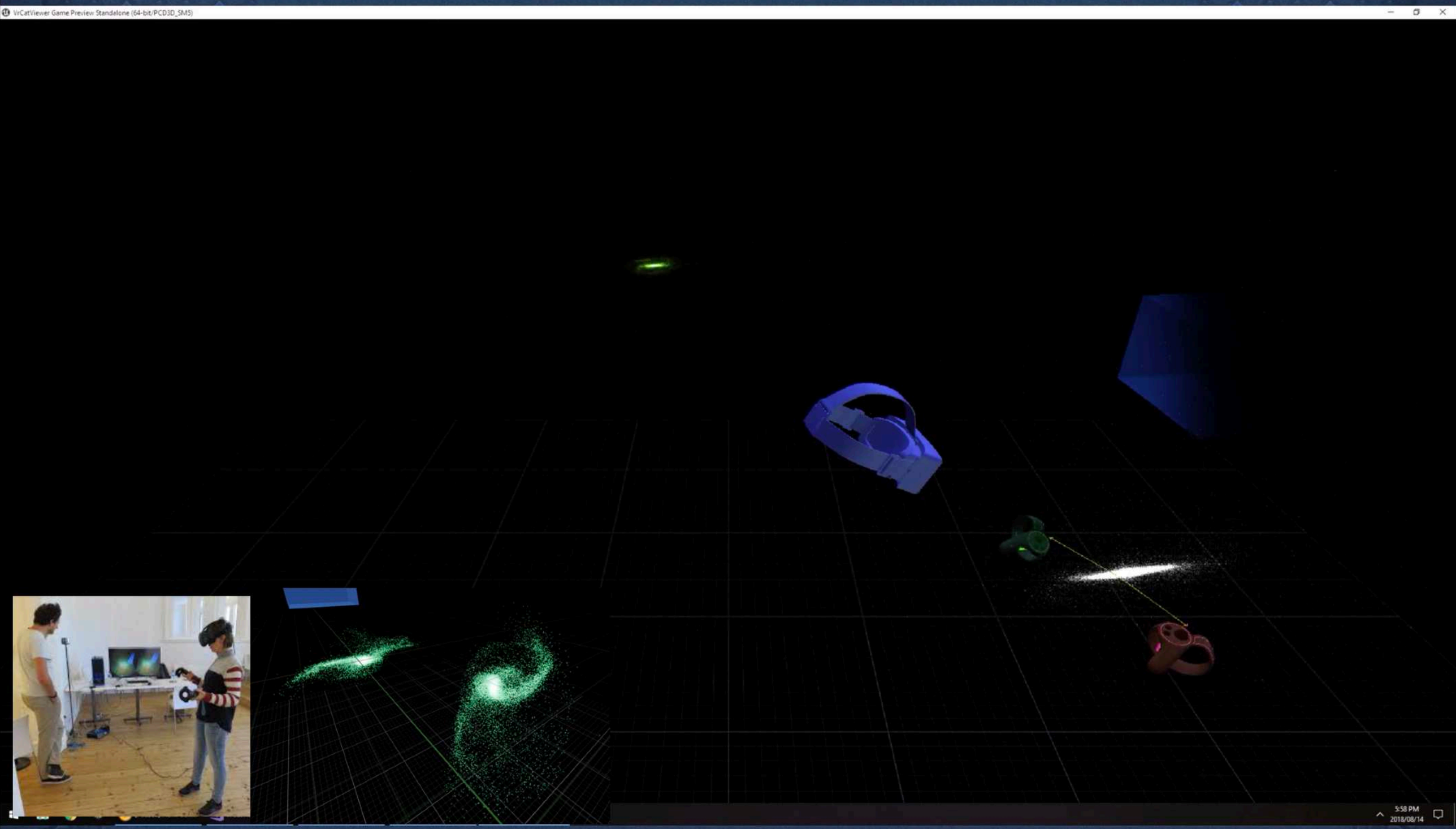

Galaxy-Galaxy Interaction (Nathan Deg 2018)

Astro VR

Galaxy-Galaxy Interaction (Nathan Deg 2018)

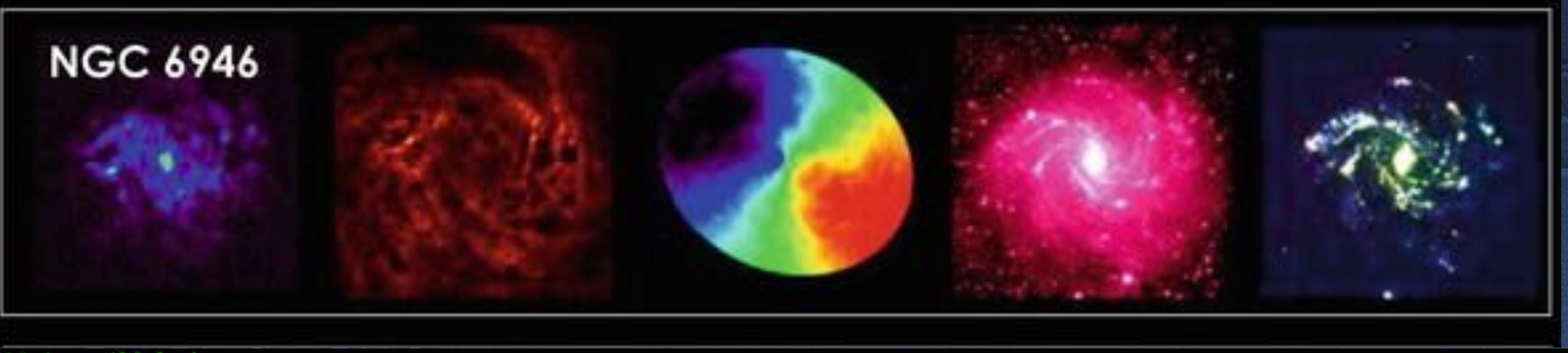

11.1 ms (90 fps)

Astro VR

Recording has started

WSRT velocity cube (Carignan+1990)

11.1 ms (90 fps)

Astro VR

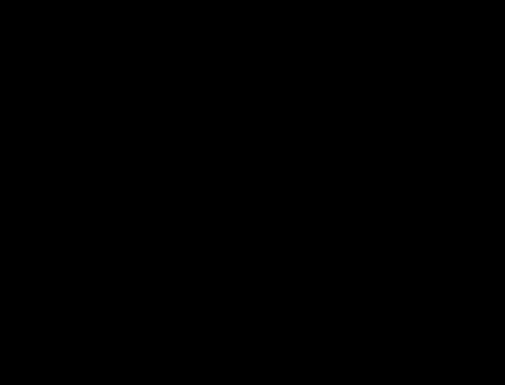

WSRT velocity cube (Carignan+1990)

11.1 ms (90 fps)

Astro VR

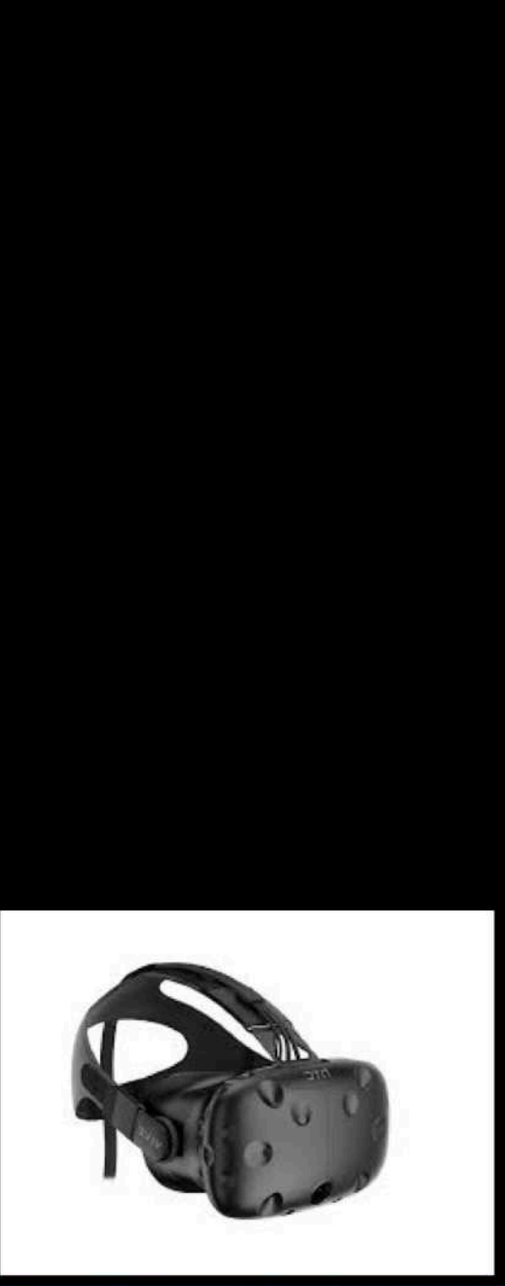

WSRT velocity cube (Carignan+1990)

UGC7766

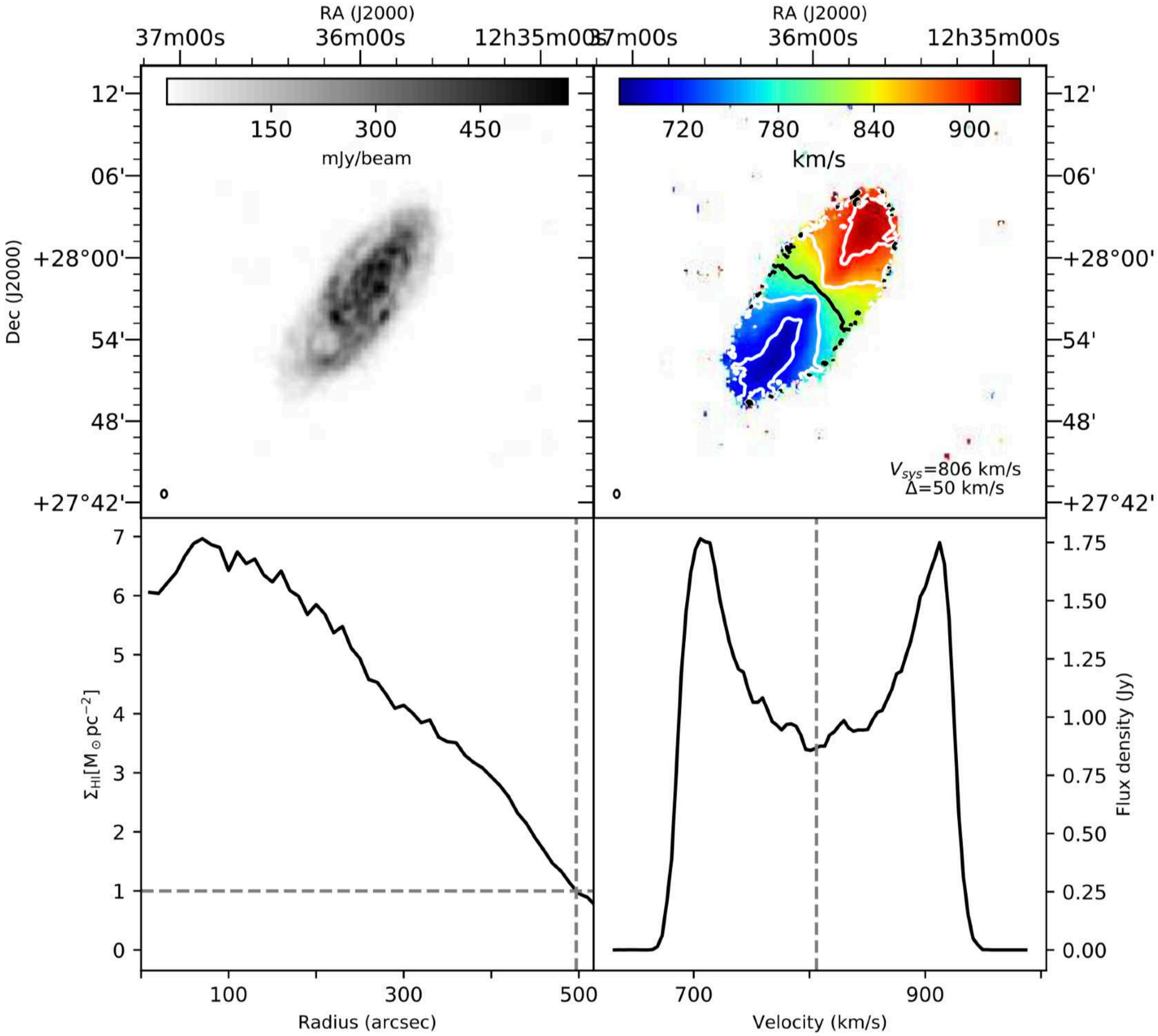
RA (J2000)
37m00s
36m00s
12h35m00s
12'
06'
+28°00'
54'
48'
+27°42'
Dec (J2000)
150
300
450
mJy/beam
720
780
840
900
km/s
V_{sys}=806 km/s
Δ=50 km/s
$\Sigma_{HI}[M_\odot pc^{-2}]$
Radius (arcsec)
100
300
500
700
900
Velocity (km/s)
Flux density (Jy)
0.00
0.25
0.50
0.75
1.00
1.25
1.50
1.75